

Simulation and Measurements of Electric and Magnetic Fields of an RFID Loop Antenna Anti-Theft Gate System

Damir Senić, Dragan Poljak, Antonio Šarolić

Original scientific paper

Abstract: The radiation of RFID anti-theft gate system based on two parallel coaxial square loop antennas has been analyzed. The system was simulated in FEKO and near electric and magnetic fields have been calculated. A physical model of the system was realized and near magnetic field was measured. Measurement results were found to be in excellent agreement with the simulation. The obtained simulation and measurement results have been compared to the exposure limits given as reference levels in the ICNIRP guidelines. No violation of limits has been shown, regarding both occupational and public exposure.

Index terms: RFID, loop antenna, gate anti-theft system, ICNIRP Guidelines, FEKO simulation, antenna measurements

I. INTRODUCTION

RFID (*Radio Frequency Identification*) is a term used for wireless recognition of object by means of radio waves. Possible areas of interest of RFID in the last years have significantly increased. Due to this fact, there are broad areas of applications: transport ID through manufacturing processes, laundry identification, authentication/verification, employee ID, access control, automated airline baggage systems, shop anti-theft protection (Fig. 1), etc [1]. RFID itself is not quite a new concept, as the same concept has been successfully used for radar identification transponders for a long time.



Fig. 1. Shop anti-theft protection gate

RFID system mainly consists of transponder (RFID tag) and reader. There are two types of RFID tags: *passive* and *active*. Passive RFID tags do not have the transmitter, as they just reflect the electromagnetic wave propagating from the reader antenna (backscatter). Active tags do have their own power supply and transmitter, which is used for broadcasting the information stored on the microchip. Passive RFID tags consist of microchip and antenna which operates at low (124 kHz, 125 kHz and 135 kHz), high (13.56 MHz) and ultra-high frequencies (860 MHz – 960 MHz and 2.45 GHz) with range up to 10 m. Active RFID tags operate at 455 MHz, 2.45 GHz and 5.8 GHz usually with range from 20 m to 100 m.

This work analyzes electric and magnetic fields radiated by an RFID reader operating at $f = 13.56$ MHz, composed of two parallel loop antennas, used in anti-theft RFID system as pass-through gate. We calculated near electric and magnetic fields using FEKO simulation software [2] based on Method of Moments (MoM). We first presented and modeled a single loop antenna, which was followed by the simulation of two parallel antennas, representing the pass-through gate. Similar study, having opened the subject, was presented in [3]. Subsequently, the pass-through gate was realized as a measurement setup, using two loop antennas. Near fields were measured and compared to the simulation results. All results were compared to ICNIRP Guidelines [4] and conclusion is given at the end.

II. LOOP ANTENNA

Loop antenna is a closed-circuit antenna type [5], [6] that may have different shapes, such as rectangle, square, triangle, ellipse, circle etc. Loop antennas can generally be divided in two different classes: antennas with conductor length and loop dimensions that are small compared to wavelength ($< \lambda/10$), and antennas with conductor length and loop dimensions comparable to wavelength. The loop antenna analyzed in this paper is considered to be a small loop antenna, behaving as a coil with constant current distribution (constant amplitude and constant phase).

The maximum of the radiation pattern is achieved in the plane of the loop. The nulls are perpendicular to the loop plane thus forming a toroidal 3D pattern. For a small square loop in xy-plane, field amplitude is given by [5]:

$$E_{\phi} = \eta \frac{\pi S I_0}{\lambda^2 r} \sin \theta \quad (1)$$

Manuscript received October 20, 2010, revised November, 2010.

This research was supported by the Ministry of Science, Education and Sports of the Republic of Croatia (Projects No. 023-0000000-3273, No. 023-0231582-1585 and No. 036-0361630-1631).

D. Senić, D. Poljak, and A. Šarolić are with the University of Split, Split, Croatia. (email: {damir.senic, dragan.poljak, antonio.sarolic}@fesb.hr).

where η is wave impedance, S is loop geometrical area, I_0 is feed current, λ is the wavelength, r is the distance from the antenna, θ is the elevation angle.

Due to their sharp nulls and broad maxima, small loop antennas are widely used for different purposes.

Matching properties of a small loop antenna can be improved by using matching elements. Due to its geometry, the antenna impedance is dominantly inductive. A capacitor is thus used as a matching element to compensate the inductive reactance. The resistive component of a small loop antenna impedance is very small. In order to match the antenna to a 50Ω line, a resistor must be incorporated in the structure.

III. SIMULATION MODELS

The loop antenna of interest for this analysis is a square loop antenna made of planar conductive strip, commonly used in RFID readers [7]-[10]. The radiated field has been simulated by using FEKO software package featuring the Method of Moments (MoM). The loop antenna dimensions were $50\text{ cm} \times 50\text{ cm}$, with strip width of 35 mm and strip thickness of 1 mm (Fig. 2). The antenna is placed in the upright position (in the vertical plane). The voltage source is positioned in the middle of the lower horizontal part of the loop. The antenna is made of copper. Antenna works at 13.56 MHz (wavelength of 22.12 m) thus fulfilling the condition for an electrically small loop antenna regarding its dimensions being smaller than $\lambda/10$.

Two different models were prepared in FEKO, starting with simple matched square loop antenna (Fig. 3) followed by simulation of gate antenna system (Fig. 4). All antennas had voltage source excitation with input power of 100 mW matched to the antenna which presents a typical input power value of common RFID anti-theft gate readers [7,8].

A series RC circuit was used as matching circuit, to annihilate the reactive impedance component and to set the real part of the antenna input impedance to $50\ \Omega$, which is the characteristic impedance of a feeding cable. Matching circuit consisted of $50\ \Omega$ resistor and 60 pF capacitor.

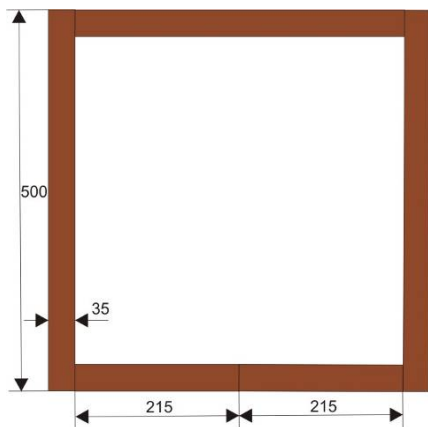


Fig. 2. Square loop antenna with dimensions in millimeters [10]

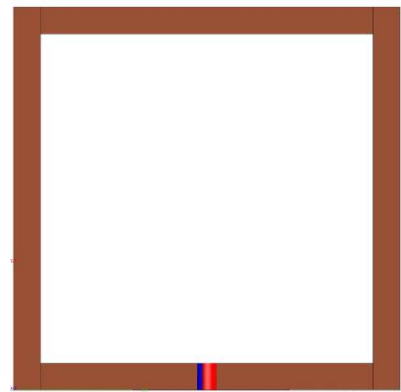


Fig. 3. Single square loop antenna with excitation

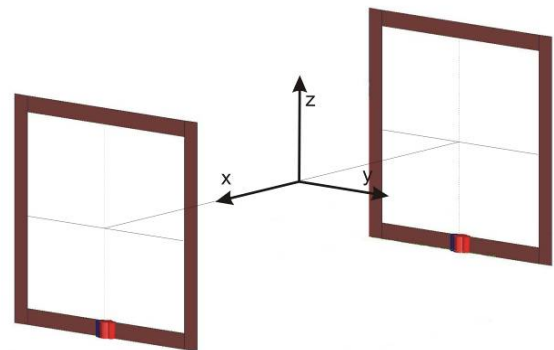


Fig. 4. Gate antenna system

IV. SIMULATION RESULTS

At the first stage, the results for a single matched loop antenna placed in yz -plane are presented. Simulated antenna had a perfectly shaped far field radiation pattern with maximum gain of 1.69 dB , shown in Fig. 5 and Fig. 6.

Further development of actual model toward the realistic one was related to the simulation of the electric and magnetic field of gate antenna system and to the comparison of the results to the exposure limits given by ICNIRP guidelines [4].

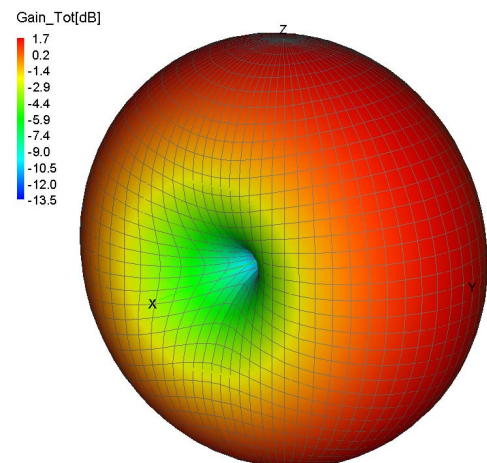


Fig. 5. Single matched loop antenna 3D far field pattern

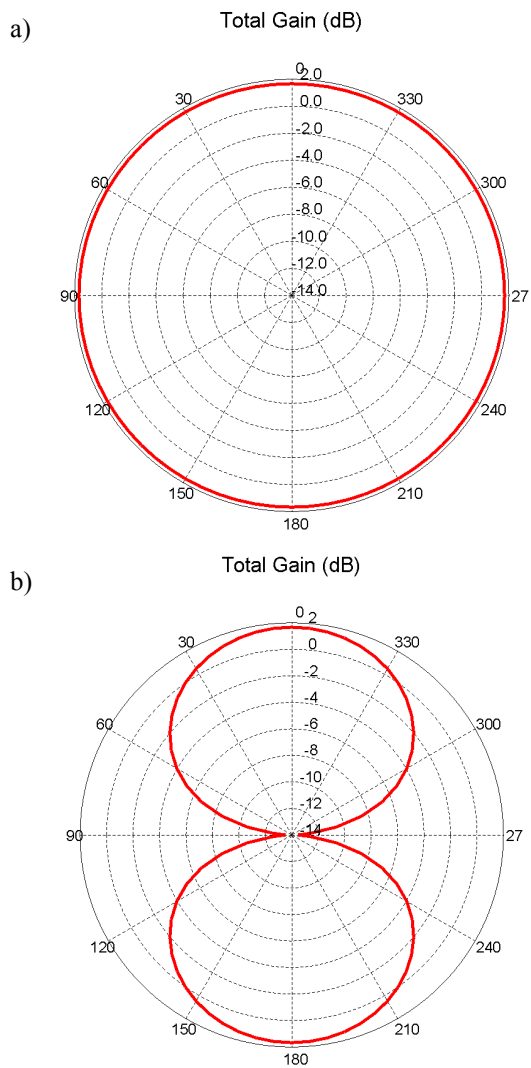


Fig. 6. Single matched loop antenna 2D far field pattern: a) yz-plane; b) xz- or xy-plane

Typical gate antenna system (Fig. 1), whose dimensions are 150 (height) × 60 (width) × 4 (thickness) cm³, consists of two identical parallel antennas. Minimum gate width is 60 cm, maximum width is 160 cm and standard gate width is 120 cm.

Simulations of the gate antenna system have been undertaken with loop separation of 60 cm, presenting the most critical (worst case) antenna configuration concerning the magnitude of radiated fields. The centre of anti-theft gate system was placed at $x = 0$, $y = 0$ and $z = 1$ m (Fig. 7). Both antennas were parallel to yz-plane.

The antennas in this simulation model differed from the model shown in Fig. 3 and Fig. 4 – they were realized with wires instead of strips, because this antenna system was subsequently realized as a measurement setup. Wires were chosen for easier physical realization.

The wire radius was chosen to be 0.9 mm. The side length of the wire square loop was fixed to 46.5 cm to achieve the same equivalent loop area as that of the previously described strip model. Thus the simulation model was adjusted to follow the physical model.

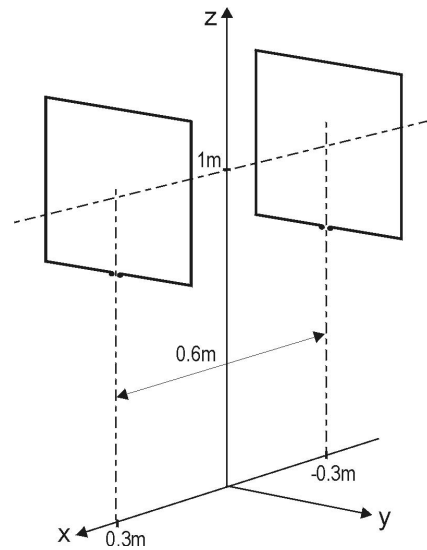


Fig. 7. Gate antenna system used for simulation and measurement

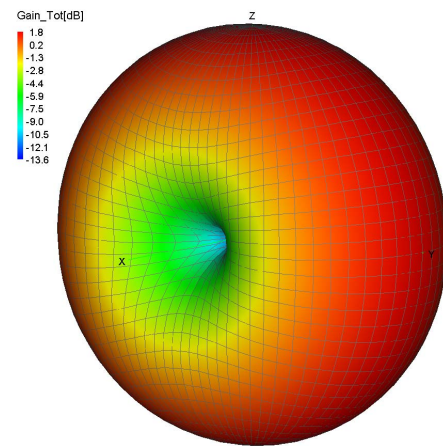


Fig. 8. Gate antenna system 3D far field pattern

The radiation pattern obtained for the gate antenna system (Fig. 8 and Fig. 9) is quite similar to previously obtained pattern for a single matched loop antenna (Fig. 5 and Fig. 6). The gain has increased to 1.8 dB.

It is very important to emphasize that the purpose of RFID loop antennas requires their use in the near field zone; RFID tags and antennas are very close to each other compared to the wavelength. Therefore, near field calculation is of interest in this analysis.

Near fields were calculated for the same model of the gate antenna system. Antennas were matched to obtain the input impedance of 50 Ω. The feeding power was set to 50 mW for each antenna, which yields a total input power of 100 mW, common in RFID anti-theft gate readers.

First, the total electric and magnetic fields between antennas along their common axis (parallel to x-axis, defined by $y = 0$, $z = 1$ m) have been studied. Simulations have show that electric field strength in the center of each loop is 2.5 V/m, falling to 1.3 V/m at the central point of the gate antenna system (Fig. 10a). The electric field changed its polarization along the axis. Although the electric far field should

theoretically be zero along this axis, the near electric field deviates from the far-field prediction. Theoretically, loop is always analyzed as continuous conductor, current flowing through it without discontinuities. The far-field of such loop placed in xy -plane is proportional to $\sin\theta$. However, real loop is fed by a voltage source, and this voltage discontinuity generates the near electric field that deviates from the far-field picture.

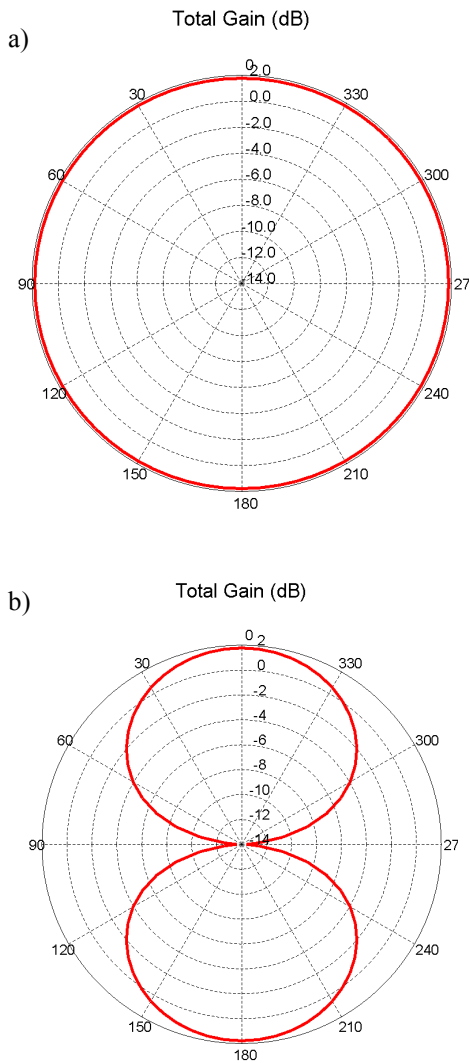


Fig. 9. Gate antenna system far field pattern: a) yz -plane; b) xz -plane

The magnetic near field shows similar behavior concerning its amplitude. Maximum value of the total field was 66 mA/m in the center of each loop, it decreased along the common axis to the central distance between antennas where it had the minimum value of 35 mA/m, increasing again toward second antenna to the same maximum value (Fig. 10b). The dominant component of the total electric field was H_x .

Results obtained in this analysis, shown in Fig. 10, comply with reference levels defined in ICNIRP Guidelines [4], opposed to the results published in [3] that showed much higher values. The reason for such a dramatic difference lies in

the applied input power. In [3], simulation was undertaken with the same input power of 100mW fed to a perfectly matched antenna. However, that model did not incorporate a matching resistor, which implies that all input power was radiated, without any losses (available option in FEKO). On the other hand, the realistic model, studied in this paper, incorporated matching elements, and thus the major part of the input power was dissipated by the matching resistor. Due to those losses, less power was radiated, generating lower field strength around the antenna. This model should correspond better to the realistic scenario.

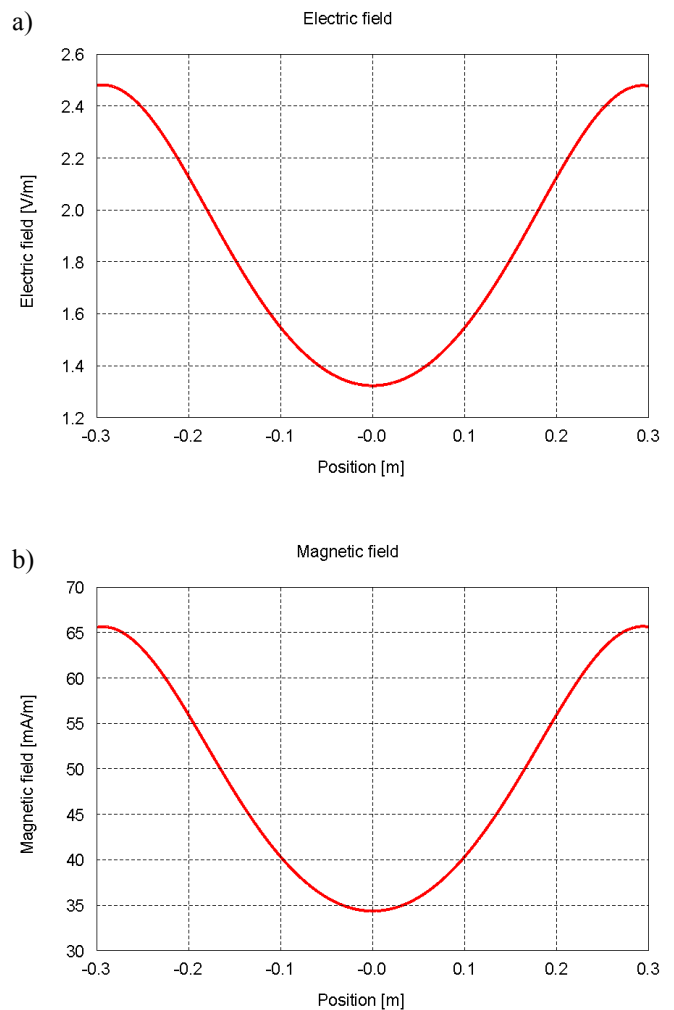


Fig. 10. a) Near electric field; b) Near magnetic field, between the antennas along their common axis (defined by $y = 0, z = 1$ m)

The next step was to calculate the near field distribution along the other axis of symmetry of the antenna system, parallel to y -axis. Near fields were calculated along the line defined by $x = 0$ m and $z = 1$ m (Fig. 11). This line refers to the pass through the gate, as it occurs in theft protection applications. Also, magnetic field distribution was calculated in the cross-section of the antenna gate system, parallel to the antennas, at $x = 0$ (Fig. 12). Both Fig. 11 and Fig. 12 show total fields, since the fields change their polarization along the axis in Fig. 11, as well as along the surface shown in Fig. 12.

V. MEASUREMENT RESULTS

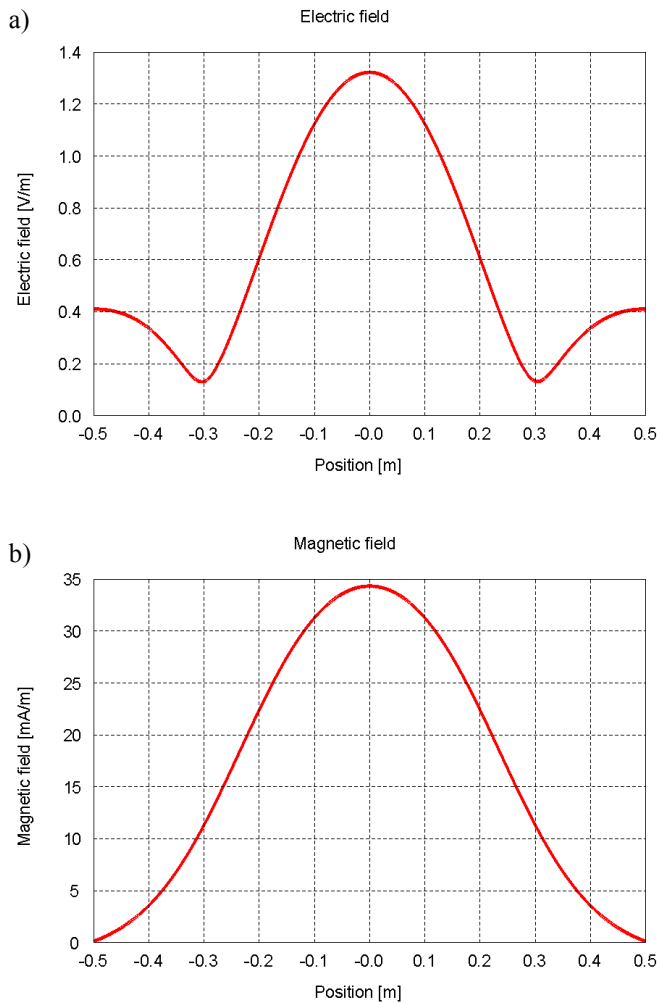


Fig. 11. a) Near electric field; b) Near magnetic field, between the antennas, along the pass-through axis, defined by $x = 0, z = 1$ m

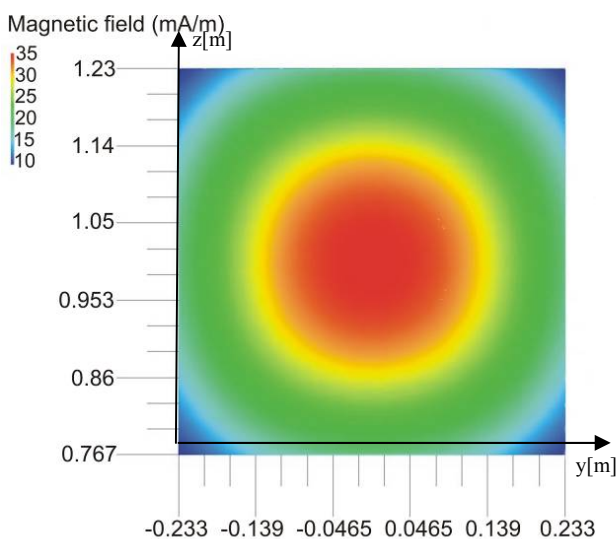


Fig. 12. Near magnetic field between antennas in yz -plane

In the previous section, the results of RFID loop antenna simulations have been presented. As the near magnetic field dominates over near electric field (as is normal in the vicinity of a magnetic loop antenna where wave impedance is smaller than that of free space) further progress was to undertake magnetic field measurements concerning studied RFID anti-theft antenna gate model. Fig. 13 shows the setup used for magnetic field measurement. Antennas were made from copper wire having radius of 0.9 mm, bent to form square loops having side length of 46.5 cm. Matching element, consisting of serial RC circuit was soldered at the top of the each antenna and the feeding 50 Ω coaxial line was connected to the bottom of each antenna. Antennas were fed from Rohde&Schwarz SM300 signal generator through a power divider. Input and reflected power was measured with Rohde&Schwarz NRP-Z21 power sensor connected to PC. Measurement results were normalized to input power of 50 mW to each antenna (total power of 100 mW) for easy comparison with the simulation results. Magnetic field was measured with own-made calibrated magnetic field probe connected to Anritsu MS2663C spectrum analyzer.

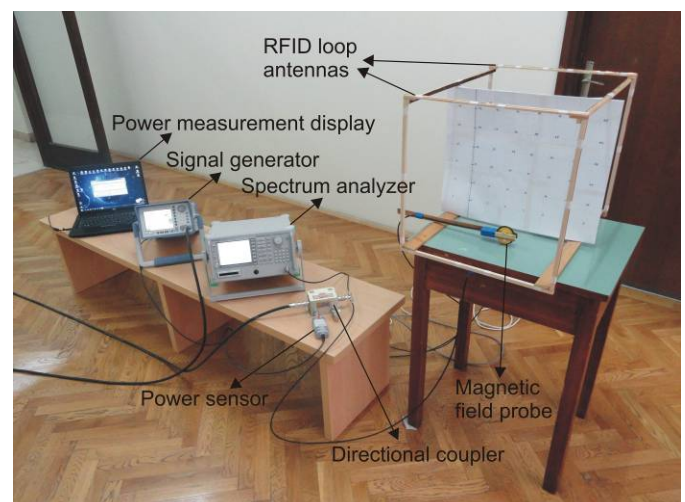


Fig. 13. Measurement setup for magnetic near field measurement of RFID anti-theft gate system

During measurements, the center of the antenna gate system was elevated 1m above the floor, which presents a typical RFID anti-theft gate reader position.

Magnetic field probe was made as a single loop with 5 cm diameter. The probe was calibrated in GTEM cell TESEQ 750, which presents a controlled electromagnetic environment having a test volume with homogenous electric and magnetic field in TEM mode. Calibration of the magnetic field probe was done using a previously calibrated isotropic electric field probe HI-4455 as a transfer standard (Fig. 14). The input signal was fed to GTEM cell at 13.56 MHz. Electric field was measured inside the GTEM cell by the calibrated electric field probe, and the actual magnetic field could be readily calculated taking advantage of TEM conditions in the GTEM cell, having the wave impedance of $120\pi \Omega$. The field was then measured at the same point by the probe under calibration.

The calibration factor was easily calculated and applied during subsequent measurements.

The measurement results of the magnetic field between the antennas along their common axis (defined by $y = 0, z = 1\text{m}$) are shown in Fig. 15. Measurements were carried out with 10 cm sampling resolution. Results are in good agreement with simulation results shown in Fig. 10b. The field consisted mainly of the x component, the other two field components were found to be negligible.



Fig. 14. Magnetic field probe calibration in GTEM TESEQ 750 cell using isotropic electric field probe HI-4455

The results of magnetic field simulation along the other axis of symmetry of the antenna system, the line parallel to y -axis, defined by $x = 0\text{ m}$ and $z = 1\text{ m}$ (pass-through axis), was verified with measurements shown in Fig. 16. Measurements were performed along the 1 m line, with sampling resolution of 10 cm. Along the gate entrance, the field level increased approaching the gate centre, where it reached the maximum value of nearly 40 mA/m and then decreased again away towards the gate exit. Achieved measurement results were again in satisfactory agreement with FEKO simulation results (Fig. 11b).

In this measurement set, all three components of magnetic field were measured and total field was contributed by all three field components. All results obtained from the measurements comply with limit values proposed by ICNIRP Guidelines for both occupational and general public exposure. Next sets of measurements refer to the magnetic field distribution along a vertical line from $z = 0$ to $z = 2\text{ m}$, corresponding to a standing human. Two measurement scenarios were carried out: first one (Fig. 17) refers to a human standing in the center of the antenna system ($x = 0, y = 0$), and the second one (Fig. 18) refers to a human standing beside the system, at a diagonal distance of approx. 1.8 m from the center of the antenna system ($x = 1.3\text{ m}, y = 1.3\text{ m}$).

The first case refers to a shop customer exposure while standing between the antennas in the anti-theft gate, which happens only for a brief period of time. The second case could refer to a shop employee working beside the anti-theft gate for a longer period, this scenario being quite realistic. Measurements were performed with sampling resolution of 10 cm. All three components of magnetic field have been measured since they all contribute to the total field strength.

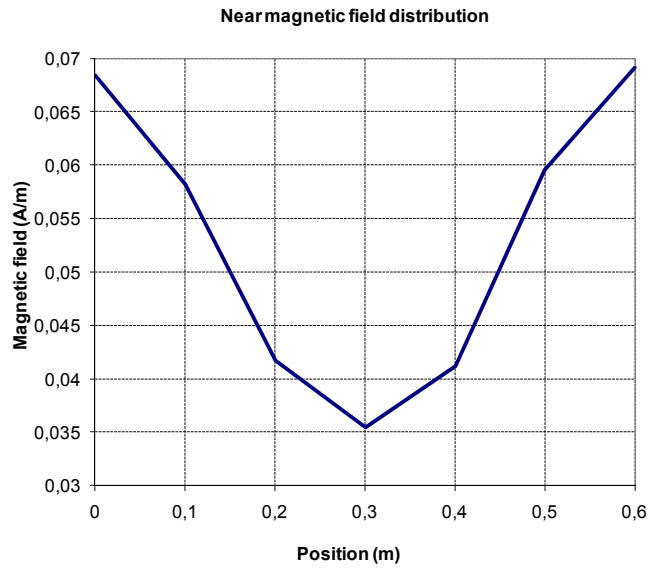


Fig. 15. Near magnetic field measurement results between the antennas, along their common axis, defined by $y = 0, z = 1\text{ m}$

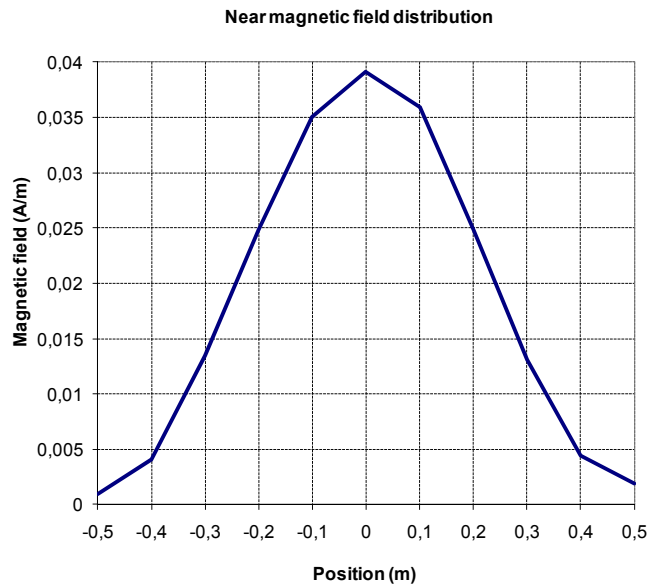


Fig. 16. Near magnetic field measurement results between the antennas, along the pass-through axis, defined by $x = 0, z = 1\text{ m}$

The maximum field level measured along z -axis (Fig. 17) was in the center of the system. Field strength decreased rapidly when probe was moved upwards or downwards from the antenna system. The field strength along the vertical line in the vicinity (but outside) of the antenna gate system (referring to potential personnel exposure) is lower than the field in the system center by at least one order of magnitude (Fig. 18).

Finally, the magnetic field distribution was measured in the cross-section of the antenna gate system, parallel to the antennas and yz -plane, at $x = 0$ (Fig. 19). Measurements were performed over $47\text{ cm} \times 47\text{ cm}$ square, whose centre is placed at $x = 0\text{ m}, z = 1\text{ m}$, with measurement resolution of 6 cm, yielding $8 \times 8 = 64$ points. Only x component of magnetic field was measured at each point due to negligible values of other two components. Results are plotted in *Matlab* and shown in Fig. 19. As expected, maximum field level was at the centre of the plane and it was approximately 35 mA/m which

is in excellent agreement with FEKO simulation results shown in Fig. 12.

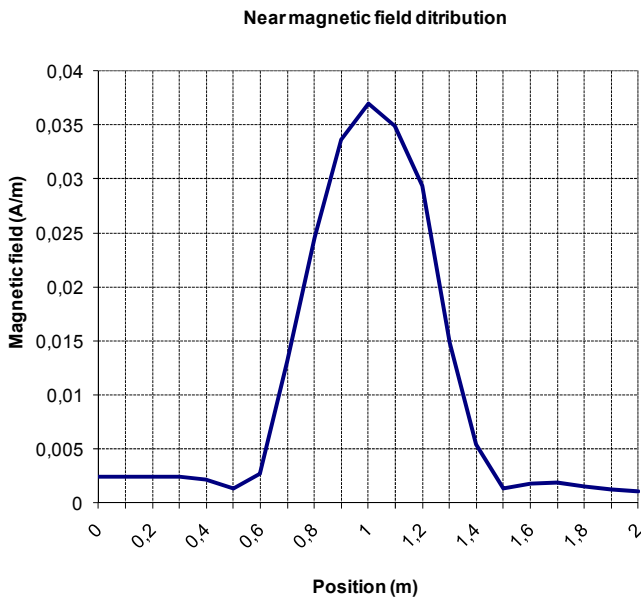


Fig. 17. Near magnetic field measurement results between the antennas along the z-axis ($x = 0, y = 0$)

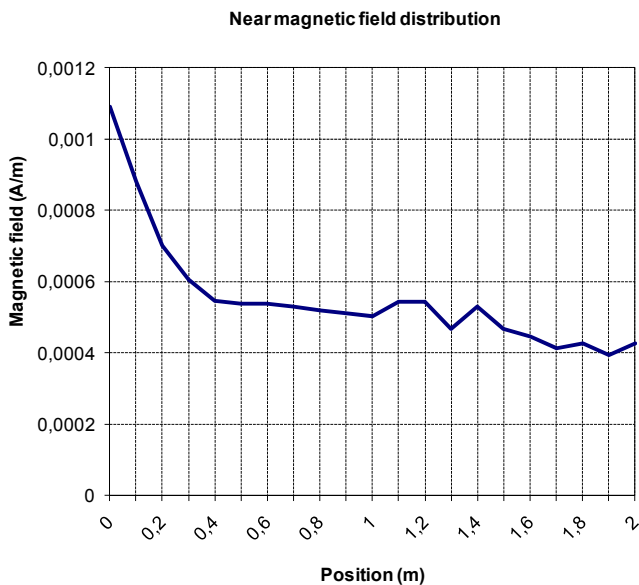


Fig. 18. Near magnetic field measurement results along a vertical line, $x = 1.3 \text{ m}, y = 1.3 \text{ m}$, from $z = 0$ to $z = 2 \text{ m}$

A final review of the electric and magnetic field maximum values obtained by simulation and measurements, as well as their comparison to the limits proposed by the ICNIRP guidelines, is given in Table I.

ICNIRP guidelines give the reference levels as limits for whole-body exposure, averaged over 6 minute time period. Considering RFID anti-theft device application, usual retention in the antenna vicinity does not last longer than few seconds. Also, the field in the system was shown to be highly non-homogenous, thus causing a partial body exposure.

Therefore, even if field strength were higher than the ICNIRP reference values, it still would not automatically implicate non-compliance. However, results showed that electric and magnetic field strength was lower than the reference levels from the ICNIRP guidelines. Consequently, no radiation hazard is expected from the analyzed device concerning whole-body exposure.

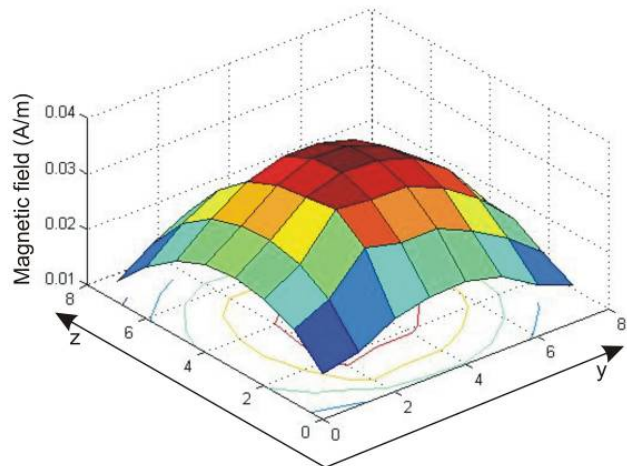


Fig. 19. Near magnetic field measurement results in the cross-section of the antenna gate system, parallel to the antennas and yz-plane, at $x = 0$

TABLE I

SIMULATED AND MEASURED NEAR ELECTRIC AND MAGNETIC FIELD STRENGTH (MAXIMUM VALUES), COMPARED TO ICNIRP GUIDELINES

Location	E-field strength [V/m] (maximum value)	H-field strength [mA/m] (maximum value)
Simulation		
along the common axis of the antenna gate	2.5	65.6
along the pass-through axis	1.3	34.3
Measurement		
along the common axis of the antenna gate	-	68.3
along the pass-through axis	-	39.1
along the vertical axis from $z = 0$ to $z = 2 \text{ m}$ (human standing in the center of the antenna gate)	-	37
along the vertical axis from $z = 0$ to $z = 2 \text{ m}$ (human standing beside the gate at the diagonal distance of 1.8 m)	-	1.1
ICNIRP guidelines [4]		
occupational exposure	61	160
general public	28	73

Eventual health risk due to malfunction of implanted devices (such as pacemakers) is beyond the scope of this paper.

VI. CONCLUSION

In this paper, the analysis of an RFID anti-theft antenna gate system has been presented, regarding its radiation and compliance to ICNIRP guidelines.

Electric and magnetic field strength was calculated using models based on square loops. Calculations were based on FEKO simulations of a single square loop antenna, and a model consisting of two identical parallel coaxial square loop antennas, forming a gate antenna system. The separation distance of 60 cm was chosen, corresponding to a worst-case configuration of a shop anti-theft device. Simulation results showed full compliance to ICNIRP guidelines, i.e. field levels were below the reference levels.

Simulations were verified with magnetic field measurements, done on a physical model of a previously described antenna gate system. Obtained measurement results showed excellent agreement with FEKO simulation results, thus confirming full compliance to ICNIRP guidelines. Field distributions have been presented graphically, showing that the human exposure between the antennas would not be uniform.

The models and results shown in this paper could contribute to a more comprehensive analysis of human exposure to RFID anti-theft systems, concerning partial body exposure and electromagnetic compatibility of implanted devices, using a realistic human model and a model of an implanted device.

REFERENCES

- [1] N. Raza, V. Bradshaw, M. Hague: *Applications of RFID Technology*, IEE Colloquium of RFID Technology, pp. 1-5, 1999.
- [2] FEKO Suite 5.5, EM Software & Systems, <http://www.feko.info>
- [3] D. Senic, D. Poljak, A. Sarolic: *Electromagnetic field exposure of 13.56 MHz RFID loop antenna*, 17th International Conference on Telecommunications & Computer Networks – SoftCOM 2010, Bol – Split, pp. 65-69, 2010.
- [4] *International Commission on Non-Ionizing Radiation Protection, Guidelines for Limiting Exposure to Time-varying Electric, Magnetic and Electromagnetic Fields (up to 300 GHz)*, Health Physics, 74(4), pp. 494-522., 1998.
- [5] C. A. Balanis: *Antenna Theory Analysis and Design*, 2nd Ed., John Wiley & Sons, New York, 1997.
- [6] J. D. Kraus: *Antennas*, 2nd Ed., New Delhi, 1997.
- [7] K. Finkenzeller: *RFID handbook*, 2nd Ed., John Wiley & Sons, Munich, 2003.
- [8] J. G. Lee, J. K. Byun, H. D. Choi, C. Y. Cheon, Y. S. Chung, B. Lee: *A New Equivalent Antenna Model for Human Body Exposed to 13.56MHz RFID System*, IEEE International Symposium on Antennas and Propagation, San Diego, pp. 1-4, 2008.
- [9] X. Qing, Z. N. Chen: *Proximity Effects of Metallic Environments on High Frequency RFID Reader Antenna: Study and Applications*, IEEE Transactions on Antennas and Propagation, Vol.55, No.11, pp.3105-3111, Nov. 2007.
- [10] S. Kong, D. Choi, H. Oh: *Evaluation of Human Exposure to Electromagnetic Fields from RFID Devices at 13.56 MHz*, Asia-Pacific Microwave Conference, Hong Kong and Macau, pp. 1-4, IEEE 2008.



Damir Senić received the Diploma Engineer degree in Electrical Engineering in 2008 from the Faculty of Electrical Engineering, Mechanical Engineering and Naval Architecture, University of Split, Croatia.

He is currently a research assistant and PhD student at the University of Split, Faculty of Electrical Engineering, Mechanical Engineering and Naval Architecture (FESB), Department of Electronics. His research interests are: electromagnetic measurements, bioeffects of EM fields, electromagnetic compatibility (EMC) and radiocommunications.



Dragan Poljak (M'96) was born in Split, Croatia, in 1965. He received the B.Sc. degree in 1990, the M.Sc. degree in 1994, and the Ph.D. degree in electrical engineering in 1996, all from the University of Split, Split.

He is currently a full-time Professor in the Department of Electronics, University of Split, and he is also an Adjunct Professor at the Wessex Institute of Technology, Southampton, Hampshire, U.K. His research interests include frequency and time-domain computational methods in electromagnetics, particularly in the numerical modeling of wire antenna structures, and recently numerical modeling applied to environmental aspects of electromagnetic fields. He has published more than 200 journal and conference papers in the area of computational electromagnetics, seven authored books and one edited book, by WIT Press, Southampton-Boston, MA, and one book by Wiley, Hoboken, NJ.

Dr. Poljak is a member of the editorial board of the journal *Engineering Analysis with Boundary Elements*, and Cochairman of the WIT International Conference on Computational Methods in Electrical Engineering and Electromagnetics. He is also the editor of the WIT Press Series *Advances in Electrical Engineering and Electromagnetics*. Recently, he has been awarded by the *National Prize for Science*.



Antonio Šarolić received the Diploma Engineer, MS and PhD degrees in Electrical Engineering in 1995, 2000 and 2004 from the University of Zagreb, Croatia. He was employed at the same university from 1995 to 2005, at the Faculty of Electrical Engineering and Computing (FER), Dept. of Radiocommunications. In 2006 he joined the University of Split, FESB, Department of

Electronics and is now Assistant Professor in Electrical Engineering. His areas of interest are electromagnetic measurements, bioeffects of EM fields, electromagnetic compatibility (EMC) and radiocommunications.